I J C T A, 6(2) December 2013, pp. 139-151

Robust CMOS Camera Module Lens Calibration by Support Vector Regression

Chan-Yun Yang*, Hooman Samani and Gene Eu Jan

ABSTRACT

An applicable paradigm motivated by the powerful computational capability in the emerging hardware for embedded lens calibration is proposed in this paper. The proposed new paradigm for the relationship between the image provider and the image processor shows functional and economical merits. The paper first focuses on the development of the embedded lens calibrator. An underlying support vector machine based regression (SVR) is hence employed as the key to achieve the goal. Based on the structural risk minimization, the SVR, employed as the calibration regressor, simultaneously minimizes both the model complexity and empirical error, and creates an estimator with a wide margin. The wide margin in regression represents a smooth approximation function for the lens calibration in which variances commonly exist in the CMOS camera modules that can tolerably be eliminated. The variance tolerability provides high robustness for the calibration function and would conduct potential success of the proposed paradigm.

Keywords: Robustness, variance, lens calibration, optical aberration, support vector regression.

I. INTRODUCTION

The online machine vision, as its importance in the robotics and automation fields, is a topic stressed on its processing speed. In a short time slice, images are repeatedly grabbed and processed in order to yield as accurate as possible perception. Plentiful image processing techniques have been invented for various purposes, such as image segmentation, feature extraction, frequency spectrum analysis, and pattern recognition but most of the techniques have been suggested to be based on an undistorted row-image for an accurate processing. As known, the image distortion (Fig. 1) mainly comes from an optical aberration, and is commonly existed in most of digital cameras which adopt only medium-level or low-level CMOS (complementary metal oxide semiconductor) camera module. Rather than a qualified post image processor dedicated for a particular image's post-processing with considerations of image distortion, a generic lens calibrator, embedded as a part of the firmware to provide first a calibrated undistorted image for the post-processing, can simplify handle the post-processing and achieve it much more efficiently.

A new architecture is suggested to establish a generalized image provider (Fig. 2) to which the source image can be readily served as undistorted as possible. With the architecture, all the image post-processors can be simplified and unified by eliminating the device-dependent image calibration. A platform across various manufacturers and devices is hence potentially sustained based on the generalization offered by the architecture.

From the market prospective, due to its compactness in volume and inexpensive in cost, CMOS camera modules (Fig. 3) are widespread among various portable device applications, such as the mobile phone, portable computer, and video recorder. Tremendous industrial modules are produced to fit the rapidly developed varieties of applications. Although the production is in large scale, the marginal profit is relatively

* Department of Electrical Engineering, National Taipei University, No. 151, University Rd., San Shia District, New Taipei City, 23741, Taiwan, *E-mail: cyyang@mail.ntpu.edu.tw; hooman@mail.ntpu.edu.tw; gejan@mail.ntpu.edu.tw*

small due to commercial competitions. The manufacturing cost, especially the cost of lens manufacturing, is hence a key to achieving a commercial success. There are diverse factors correspond to the precisions of a lens in its plastic injection manufacturing process, such as temperatures for mold and the melting polymer materials and pressures for supplying materials and injection. Despite the controls of these processing factors are often precisely and carefully taken, variances in the produced lens surface are still difficult to avoid.

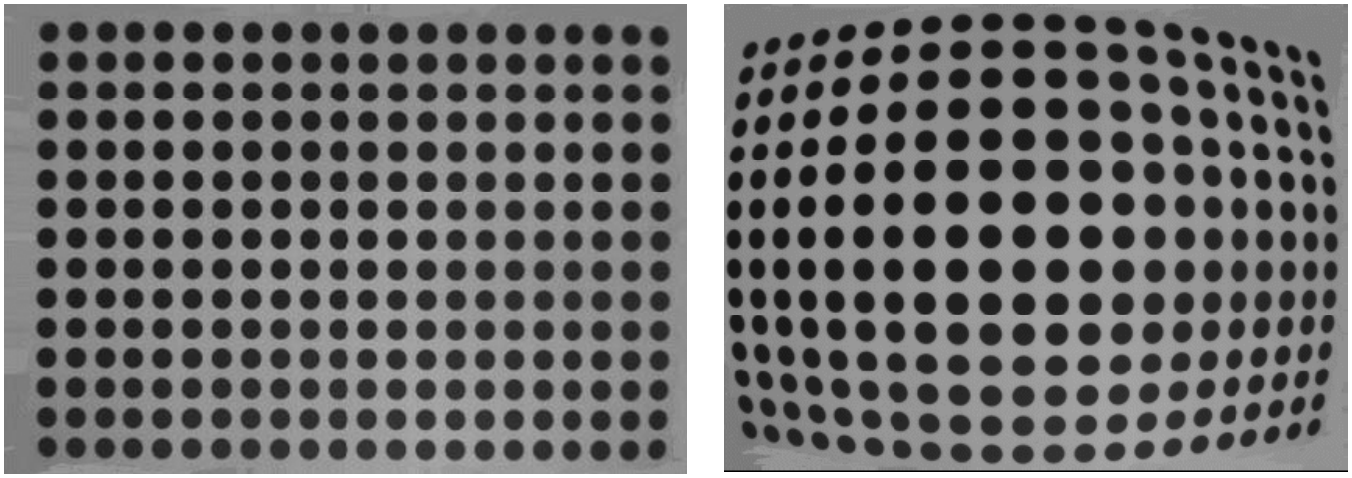

Figure 1: Image Distortion Comes from the Optical Aberration

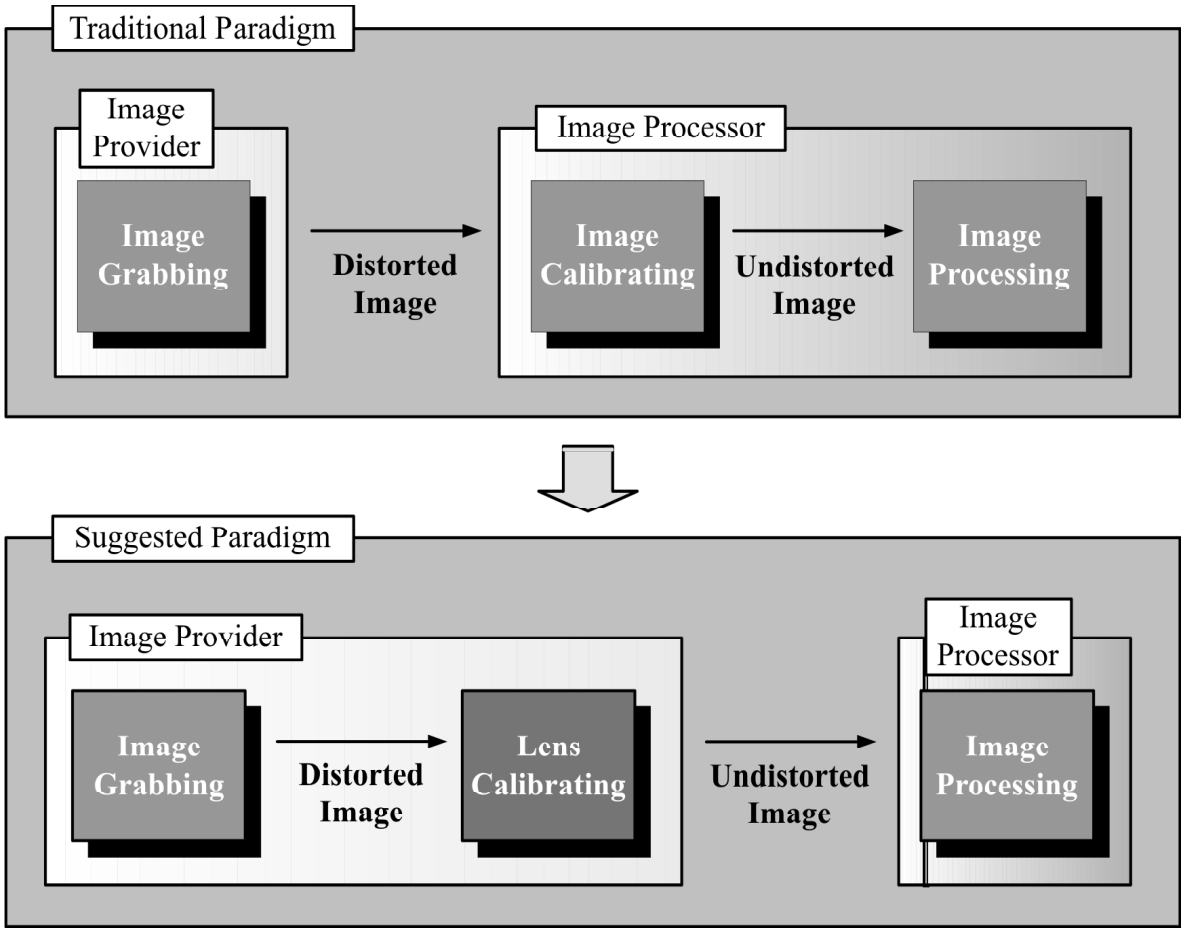

Figure 2: A Paradigm Shift for the Relationship between Image Provider and Image Processor

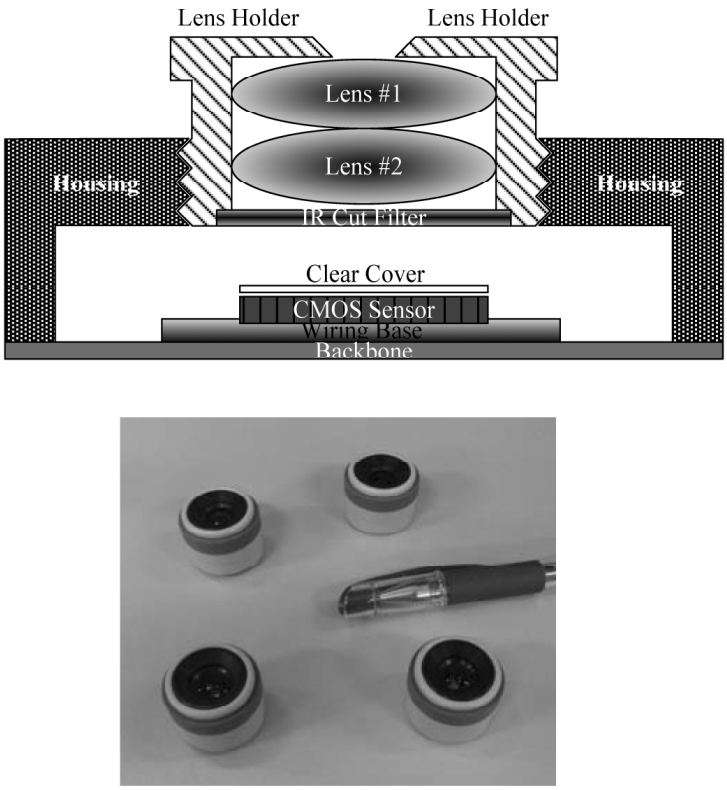

Figure 3: CMOS Camera Modules

In fact, the lens distortion is commonly existed in the inexpensive plastic-made lens. The distortion would be more serious when the lens applied in a wide-view-angle photography. The lens calibration is hence employed to recover the distortion. An undistorted image, either a standalone still image or a snapshot extracted from a streamed dynamic video, can be fully restored by an exact calibration of the corresponding lens. With the production variances mentioned above, there is a dilemma of choosing one exact calibration function to fit a lot of lenses even if their processing factors are carefully controlled. In this regard, the lens calibrator is seriously suffered from the variance device by device.

In order to fit these lenses with diverse variances, a tolerable calibration function is proposed in the study. Tracing backward to its technical nature, the lens calibration by a linear or nonlinear function is intrinsically a regression problem. Unlike a particular regression function generated for calibrating one certain lens, the regression proposed for the tolerability is dedicated to the generality and robustness for calibrating a cluster of lenses with the slight variances. The tolerability in this study is generated from a large margin support-vector-machine regression (SVR). By solving with an optimization objective function, SVR is indeed a good solution to balance the trade-off between the calibration accuracy and the corresponding tolerability. Since the variances are a nature of the lenses despite of the precision of the manufacturing process, the tolerable calibration function, instead of a particular dedicated calibration function, deserves more attention.

II. LENS CALIBRATION

The lens calibration, as its significance in the machine vision, is an inversed manipulation measuring the photogrammetric distorted image to estimate its undistorted correspondence. For variant purposes, a lot of methods of calibration have been developed to solve the distortion problem [1-3]. The study here focuses on the most common algebra approaches for an estimation of the distortion. The calibration is realized by devising mechanically a rigid calibration platform (Fig. 4) for gauging reliable points coordinates, say data

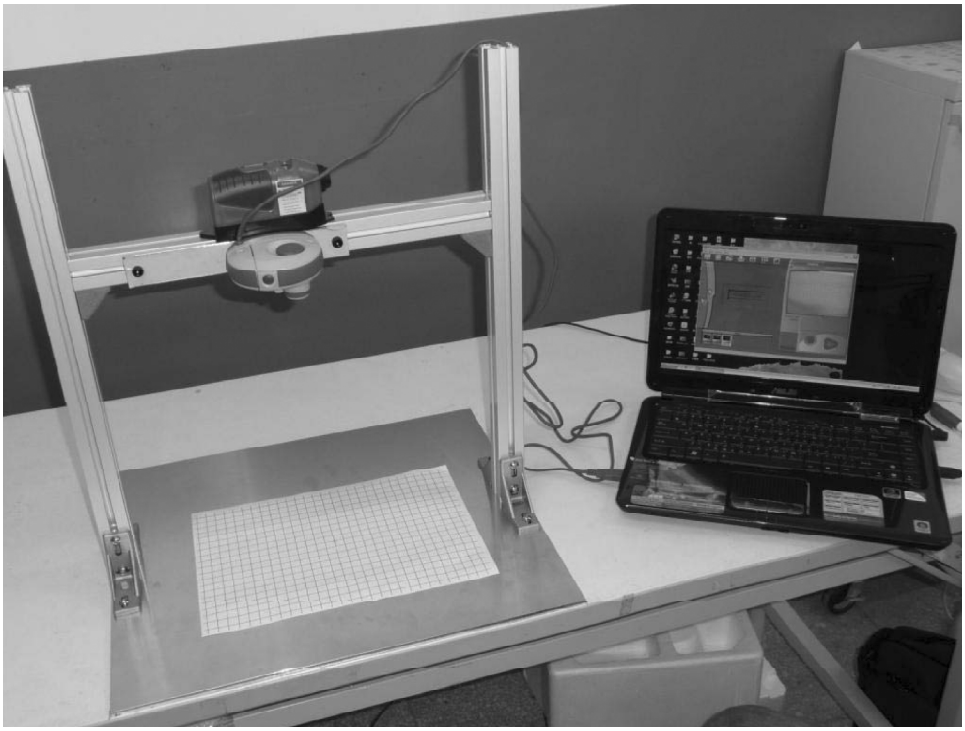

Figure 4: The Devised Rigid Calibration Framework

points, of the calibration target which is generally a two-dimensional board with parallel and perpendicular lines drawn on it. The flat board is placed parallel with the focal plan of calibrated cameras. With such a fixture platform, the calibration target can be imaged to provide correspondences between a cluster of two-dimensional distorted image point coordinates (x_d, y_d) and their corrected point coordinates (x_u, y_u). A calibration function is hence defined as a relationship function between these (x_d, y_d) and (x_u, y_u):

$$x_u = f_x(x_d), \text{ and } y_u = f_y(y_d), \tag{1}$$

where f_x and f_y are the inversed functions for recovering corrected data points (x_u, y_u) from their distorted correspondences (x_d, y_d).

The recovery intrinsically is a regression problem. Due to the difficulty to obtain 24 an exact solution, the recovery in general could only be estimated by a regression function which would be optimized by the input data points (x_d, y_d). Plainly speaking, the problem can only be solved by the observations themselves.

Tsai [4-5] has proposed a famous calibration model, beginning with the problem of lens calibration,. With the image coordinate system centered at the image center (x_c, y_c), the distortion is assumed to be radial symmetric and exaggerated extensively outward along the radial axes from the center (Fig. 1). Due to the centered symmetry, Tsai's model first converted the image point coordinates (x_d, y_d) on the projected plane from the centered Cartesian coordinate system to a polar coordinate system, and measured their radial distances r_d. The undistorted point coordinates (x_u, y_u) can thus be recovered by:

$$x_u = x_d (1 + ar_d^2), \text{ and } y_u = y_d (1 + ar^2), \tag{2}$$

where

$$r_d = \sqrt{x_d^2 + y_d^2}. \tag{3}$$

In the expressions, a is a calibration coefficient for fitting the conversion. Tsai's model here can be regarded as a polynomial regression. Devernay and Faugeras have extended the idea of Tsai by considering more the decentering and the tangential distortion, and reformulate the model as [6]:

$$x_u = x_d + a(x_d - x_c)r_d^2, \text{ and } y_u = y_d + a(y_d - y_c)r_d^2 \tag{4}$$

where

$$r_d = \sqrt{\left(\frac{x_d - x_c}{s}\right)^2 + (y_d - y_c)^2}. \tag{5}$$

In the expression, s denotes the image aspect ratio practically corresponding to the tangential distortion for adjusting the image coordinate system. Under the assumption of centered radial symmetry, the model can further be abbreviated as:

$$r_u = r_d(1 + ar_d^2). \tag{6}$$

where $r_u = \sqrt{((x_u - x_c)/s)^2 + (y_u - y_c)^2}$. It should be noted that Eq. (6) indicates that r_u is a third-order polynomial function of r_d. Haneish and Miyake [7] adopts a decentered polar coordinate system to generalize both the models of Tsai and Devernay and Faugeras as a power series. Using the power series together with polar radius r_d of the data points, the polar radius r_u of the corrected point coordinates (x_u, y_u) can be recovered by:

$$r_u = r_d + a_1 r_d^2 + a_2 r_d^3 + \cdots a_n r_d^{n+1} \tag{7}$$

Obviously, their model adopts a general high $(n + 1)$-order polynomial regression for fitting the relationship of r_u and r_d. Actually, considering the trade-off between computational complexity and the calibration precision, a sufficient second or third order polynomial is suggested. Based on above models, we are surely to admit that the adoption of linear polynomial regression models for lens calibration is intuitively excellent in both theory and application. Practically, the models are widely spread in many real-world applications.

For such a generalized polynomial model, the vector of calibration coefficients $a = [a_1, a_2, \ldots, a_n]^T$ is often obtained accordingly by a least squares optimization. For example, for a third order polynomial $r_u = r_d + a_1 r_d^2 + a_2 r_d^3$, the calibration coefficients would be $a = [a_1, a_2]^T$, $n = 2$. If the model is calibrated by a 12x12 image data points (x_d, y_d), i.e., we have $m = 144$ inputs to estimate these two calibration coefficients. The problem is thus typically well-posed due to $m >> n$, can be solved satisfactorily.

Considering extensively the decentering, tangential distortion, and thin prism distortion, Wei and Ma have developed a model more precise to the calibration [1]. By deriving first the distortion on CMOS sensor focal plane:

$$x_i = x_d + \delta^{(x)}(x_d, y_d), \text{ and } y_i = y_d + \delta^{(y)}(x_d, y_d), \tag{8}$$

where

$$\begin{cases} \delta^{(x)}(x_d, y_d) = k_1 x_d (x_d^2 + y_d^2) + (p_1(3x_d^2 + y_d^2) + 2p_2 x_d y_d) + s_1(x_d^2 + y_d^2) \\ \delta^{(y)}(x_d, y_d) = k_1 y_d (x_d^2 + y_d^2) + \underbrace{(2p_1 x_d y_d + p_2(3x_d^2 + y_d^2))}_{Decentering\ \&\ tangential\ distortion} + \underbrace{s_2(x_d^2 + y_d^2)}_{Thin\ prism\ distorition}, \end{cases} \tag{9}$$

where $\delta^{(x)}$ and $\delta^{(y)}$ are distortions corresponding to the x and y axes, respectively, and k_1, p_1, p_2, s_1, and s_2 denote respectively a set of constants corresponding to each effects from decentering, tangential distortion, and thin prism distortion, respectively. According to the distortions in Eq. (8), the corrected point coordinates (x_u, y_u) can be given by:

$$x_u = \sum_{0\le i+j\le 3} a_{ij}^{(1)} x_d^i y_d^j \Big/ \sum_{0\le i+j\le 3} a_{ij}^{(3)} x_d^i y_d^j, \text{ and } y_u = \sum_{0\le i+j\le 3} a_{ij}^{(2)} x_d^i y_d^j \Big/ \sum_{0\le i+j\le 3} a_{ij}^{(3)} x_d^i y_d^j. \tag{10}$$

The calibration coefficients $a_{ij}^{(k)}$ in the above expressions extensively become a matrix and can be arranged as:

$$A = \begin{bmatrix} a_{33}^{(1)} & ..., & a_{00}^{(1)} \\ a_{33}^{(2)} & ..., & a_{00}^{(2)} \\ a_{33}^{(3)} & ..., & a_{00}^{(3)} \end{bmatrix}. \tag{11}$$

Equivalently, the model of Wei and Ma is still a generalized third order linear polynomial.

According to the radial symmetry of the lens distortion, Smith *et al.*, [8] have directly derived a set of recursive orthogonal Chebyshev polynomials on the polar coordinate system for the calibration. The coefficients a_j of the Chebyshev polynomials are recursively computed first by the next Eqs. (12) and (13):

$$a_j = \sum_{i=0}^{m-1} r_{di}\ p_j(i) \Big/ \sum_{i=0}^{m-1} [p_j(i)]^2 \tag{12}$$

$$p_j(i) = \sum_{k=0}^{j} (-1)^k \binom{j}{k} \binom{j+k}{k} \frac{i^{(k)}}{(m-1)^{(k)}}, \tag{13}$$

and are used for interpolation, where $i = 0, 1, \ldots, m\text{-}1$ is the index of the input data 10 points, p_j, $j = 0, 1, \ldots, n$, is the j-th order of Chebyshev polynomial basis, and $i^{(k)} = i(i-1)(i-2) \ldots (i-k+1)$. Using a_j from Eq. (12), the recovery of r_u can be done 12 by:

$$r_d = \sum_{j=0}^{M} a_j p_j(r_u / b), \tag{14}$$

where b denotes a scaling constant for conversion between the input and output coordinates. At this point, we can summarize that the lens distortion is mainly resolved by a regression function, particularly a generalized algebraic polynomial functions, though all the functions have been developed significantly different. It should be noted that the Runge's phenomenon [9], which is commonly existed in an interpolation problem, is still present in such kinds of regressions since they are intrinsically an interpolation problem. The use of orthogonal Chebyshev polynomials can significantly reduce the Runge's phenomenon in the interpolations.

III. MODEL SELECTION

The next step is the admissibility of this type of algebraic polynomial regression for the before-ahead device-independent lens calibrator embedded in the image-provider. As stressed, the diverse variations are a great challenge in devising the embedded lens-calibration. In general, the higher order of a polynomial is the higher flexibility it can be for the calibration, and the higher capability for reflecting the local curvature discontinuity of surface smoothness. Whereas a higher order polynomial can precisely adapt the local curvature discontinuity, a lower one is more tolerable to the diverse variations due to the less model complexity. There is obviously a trade-off between the precision adaption and the variation tolerability. The trade-off made the model-selection of our topic different from those of the previous researches, and involved it into the model complexity [10]. The model, considering mainly the diverse variations generated by the production process, must be robust enough to resist the individual variations, and to expand essentially the most general curvature of the lenses surface. A regularized optimization model, which is beneficial

from the model-complexity penalty can deal with the trade-off well, is hence suggested for the calibration work.

IV. SUPPORT VECTOR MACHINE REGRESSION

SVM (support vector machine), founded by Vapnik *et al.* [11-12] since 1997, is a feasible alternative to traditional artificial neural networks (ANN's). The category of SVM based regression, namely termed as SVR, also has been invented for function approximation since 1998. Built on the structural risk minimization, the SVM based methods for both the classification and regression simultaneously minimize both the model complexity and empirical error, and create an estimator with a wide margin. The wide margin in regression represents a smooth approximation function in which individual variance has been rejected as much as possible. In contrast to an algebraic polynomial or an ANN regression model which devises the approximation function by only minimizing the training error between observed and corresponding predicted responses, the SVR attempts to minimize a generalization error which combines the training error and a regularization term for controlling the model complexity. The generalization error rejects mainly the highly variant noise, and achieves a rigid regression. Hence, a SVR-based embedded calibrator is proposed for the study which is sought to mostly reject the distortion variances commonly existed in the CMOS camera modules.

Based on a regularization form, SVR regresses a cluster of data points considering not only the empirical errors but also the regularized penalties to reduce the model complexity [13]. The general regularization form can first be expressed as:

$$\arg\min_{f \in H} \lambda_{\Omega} \Omega[f] + R_{emp}[f], \tag{15}$$

where $R_{\text{emp}}[f]$ denotes a summated empirical training error by measuring individual output error of all the training data points [13-14]. Together with a scaling factor λ_{Ω}, a regularization term $\Omega[f]$ has been introduced for regularization. In the expression, H denotes a reproducing kernel Hilbert space (RKHS) which is a high dimensional space mapped from the finite dimensional input data space by a kernel function $\kappa(\cdot, \cdot)$. In H, a sophisticated nonlinear problem can be solved linearly by the kernel function [14]. The model seeks to simultaneously minimize both the regularized objective and the empirical risk. With the scaling factor λ_{Ω}, the model complexity can easily be regularized. For our calibration example, the regularization term of the one-dimensional regression function $f(\mathbf{x})$ was chosen as:

$$\Omega[f] = \frac{1}{2} \| w \|^2 \tag{16}$$

with the m-length input $\mathbf{x} = [x_1, x_2, \ldots, x_m]^{\mathrm{T}}$. The regularization term corresponding to the margin $\mathbf{w}$ is a key usually used for the excellent capability of noise tolerable, and the model complexity [10]. To cope with the penalization, an ε-insensitive loss function $\xi = \max(|e| - \varepsilon, 0)$ (Fig. 5a) is introduced to convert the individual empirical errors into their corresponding slack variables $\boldsymbol{\xi} = [\xi_1, \xi_2, \ldots, \xi_m]^{\mathrm{T}}$ and $\overline{\boldsymbol{\xi}} = [\overline{\xi}_1, \overline{\xi}_2, \ldots, \overline{\xi}_m]^{\mathrm{T}}$. These slack variables here are utilized to approximate the function with certain degree of precision by a minimization scheme. A complete primal form of the SVR 11 thus can be given as:

$$\min_{\mathbf{w}, \xi, \overline{\xi}} \frac{1}{2} \| \mathbf{w}^2 \| + \lambda \sum_{i=1}^{m} (\xi_i + \overline{\xi}_i), \tag{17}$$

subject to

$$\begin{aligned} & y_i - \langle \mathbf{w}, \mathbf{x}_i \rangle - b \le \varepsilon + \xi_i, \\ & \langle \mathbf{w}, \mathbf{x}_i \rangle + b - y_i \le \varepsilon + \overline{\xi}_i, \text{ and} \\ & \xi_i, \overline{\xi}_i \ge 0, \quad i = 1, \ldots, m, \end{aligned} \tag{18}$$

where λ converting the scaling factor λ_Ω, is used to weight the balance between the regularized objective term and the empirical risk term, the expression <·, ·> represents a similarity measure which the kernel function κ(·, ·) is often taken into account, and the parameter ε for ε-insensitive loss function is used to construct a ε-tube (Fig. 5b) for controlling the error tolerability. The use of the ε-tube is to vanish its penalty of an input data point if it locates within the ε-tube. Due to the penalty vanish, the insensitive range [–ε, +ε] contributes remarkably to the smoothness of the regression function, and takes effect on the determination of number of the support vectors (*SV*) which are essential data points to sufficiently and necessarily support the output function. By taking Lagrangian with Lagrange multipliers $\alpha = [\alpha_1, \alpha_2]^T$ and $\bar{\alpha} = [\bar{\alpha}_1, \bar{\alpha}_2]^T$, the problem (17)-(18) can be converted into a dual convex quadratic problem [14-15]:

$$\max_{\alpha,\,\bar{\alpha}} -\frac{1}{2}\sum_{i,j=1}^{m}(\bar{\alpha}_i-\alpha_i)(\bar{\alpha}_j-\alpha_j)\left\langle \mathbf{x}_i,\mathbf{x}_j\right\rangle -\varepsilon\sum_{i=1}^{m}(\bar{\alpha}_i+\alpha_i)+\sum_{i=1}^{m}y_i(\bar{\alpha}_i-\alpha_i), \tag{19}$$

subject to

$$\sum_{i=1}^{m}(\alpha_i-\bar{\alpha}_i)=0,\ \textit{and}\ \ \alpha_i,\bar{\alpha}_i\in[0,\lambda],\ \ \forall i. \tag{20}$$

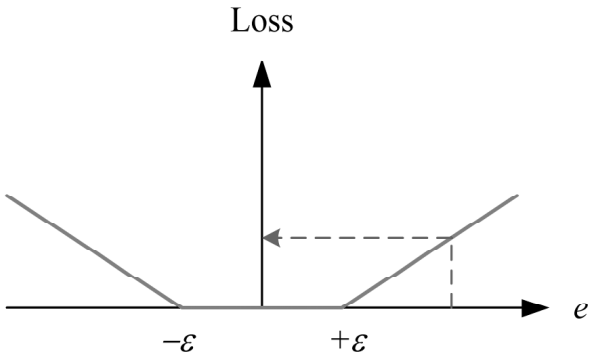

(a) Loss function

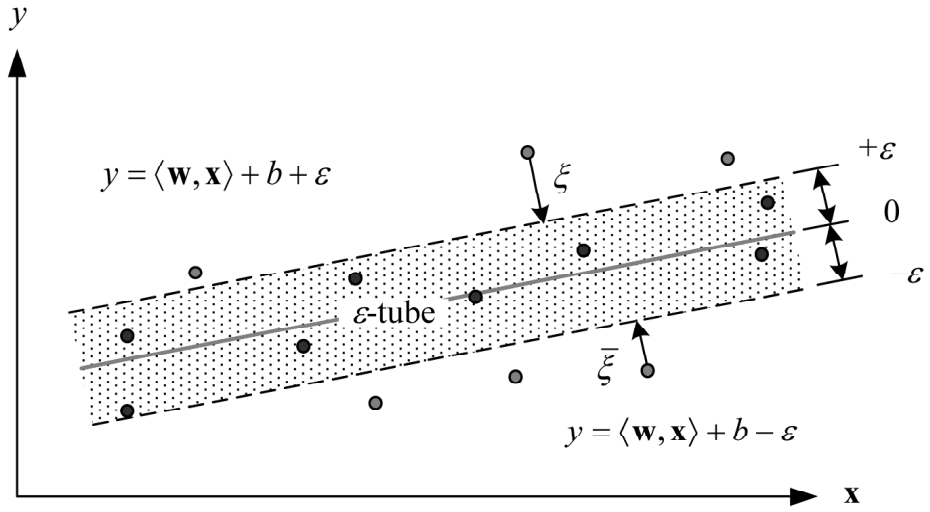

(b) ε-tube

Figure 5: Loss Function and ε-tube

Only those nonzero optimized α^* and $\bar{\alpha}^*$ are gathered to form the support vectors. The intrinsic sparseness of the support vectors has merits to speed-up the computation of interpolation using the consequent regression function. Eventually, with *SV*, the consequent regression function can be given by:

$$f(\mathbf{x}) = \sum_{x_i \in SV} \left(\bar{\alpha}_i^* - \alpha_i^*\right) \langle \mathbf{x}_i, \mathbf{x} \rangle + b. \tag{21}$$

V. RESULTS AND DISCUSSIONS

In our experiments, five CMOS camera modules for the purpose of convincing the distortion and its variations were collected for experiments. By center-aligning to a two-dimensional equally spaced grids (Fig. 1a) on the target board, which was fixed on the devised calibration platform (Fig. 4), each camera module was consecutively mounted onto the platform with an identical posture to capture the image. The calibration platform in the experiments is an important fixture to guarantee the images from different camera modules are varying only with the camera modules (lens) itself. The grids on these images were then discretized into image point coordinates (x_d, y_d) to form five set of data points, Lens#1 to Lens#5. An overlapped observation of these five sets of (x_d, y_d) is depicted in Fig. 6. A phenomenon of barrel distortions can be easily be confirmed by the observation.

The observation of the overlapped (x_d, y_d) then moves to the diverse variations of the distortion. As shown, variances exist around every (x_d, y_d). The variances of every batches of (x_d, y_d) is cylindrically distributed and expands radically in a regular and consistent tendency outward from the image center with different growing rates. The tendency reveals a dependency between the variations of distortion and the lenses. The dependency implies that the variations varying the lenses may be rooted once the lens is produced.

In our first experiment, we have collected all the data points (x_d, y_d) as the input for regression, but it failed due to a wide-spread of variations. As we found, the expanding rate of the distortion variance of a certain lens are incoherent cylindrically in every directions ranged from 0 to 2π. The fact made the regression to pay much more effort to deal with the incoherency than that to deal with the variation for maintaining the predictive accuracy. A strategy subdividing the cylindrical $0 \le \theta < 2\pi$ directions into 8 partitions, as shown the subdividing radial blue lines in Fig. 6, was thus adopted to specify the incoherency and go forward our analysis. The subdivided-partition strategy indeed took effect in depressing the incoherency. Instead of the full range of θ, the first 1/8 partition, ranging from 0 to $\pi/4$, was hence elicited for experiments and discussions.

Using the data points gathered from the first partition, the relationship of r_d is charted in Fig. 7. By different colored symbols, the relationships in every datasets show consistently an increasing tendency of larger variance of the distortion which we have stressed above, and, also, the tendency shows the so called incoherency among the datasets. With such an incoherency in variations, regression functions from both SVR and an algebraic polynomial regression are generated to fit the data points. As a delegate to represent such a noisy relationship, the regression functions for sure should be robust enough to resist to the noise. To test the robustness, a cross-validation scheme, randomly chosen a dataset for training and validated the performance with the remaining datasets, was hence selected to test the robustness of the regression functions. Here, dataset Lens#5 was chosen as the training set. With the predetermined β-order polynomial kernel function, a series of experiments were taken to find an optimized SVR function which fitted most the data points of Lens#5. By a parameter searching scheme, a low-complexity model parameterized with arguments $C = 1$, $\varepsilon = 2$, and $\beta = 2$ was eventually selected for comparison. The model with $\beta = 2$ equivalent to a 2nd order polynomial function satisfies the original expectation of low model complexity. Therefore, a curve obtained by this selected SVR function together with a comparative stump generated by a second order algebraic polynomial regression were depicted in Fig. 7 as those characterized by a black solid and a red dash lines, respectively. The proximity of these two curves show the calibration capacity the regression functions can achieve would be very close.

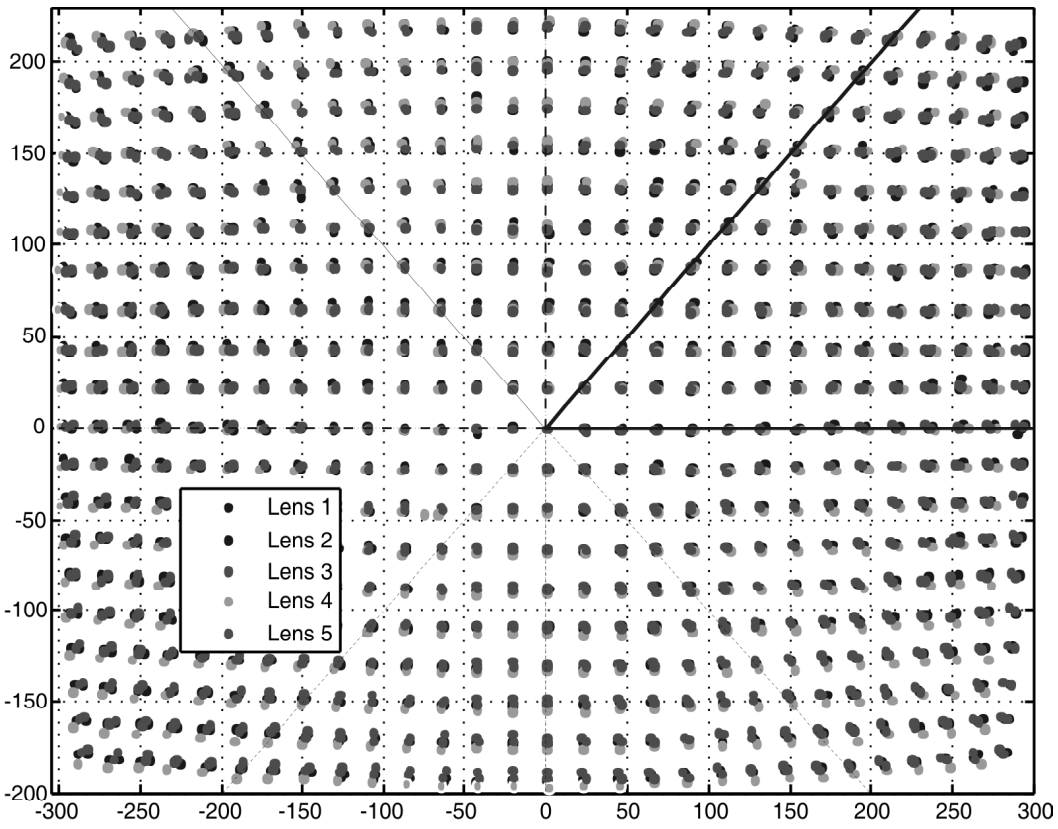

Figure 6: Distorted Grid-map from Different Lenses

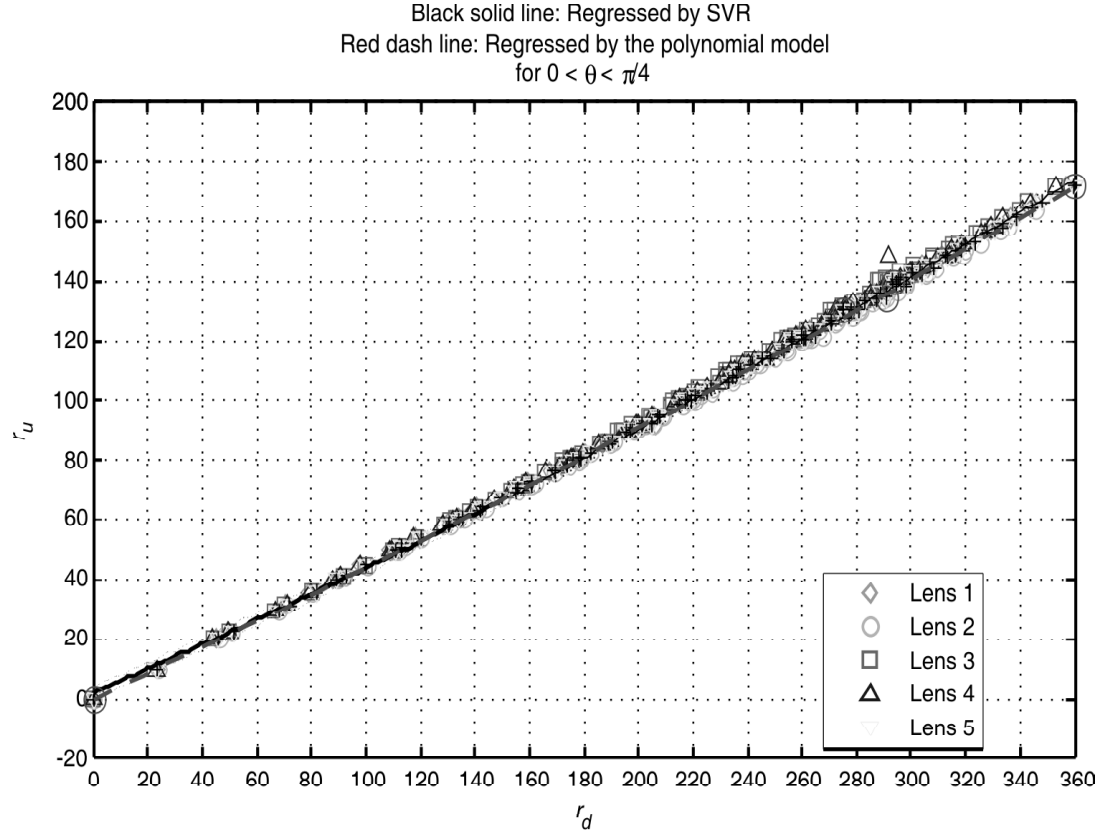

Figure 7: Regression Functions Generated by SVR and a 2nd order Algebraic Polynomial Regression with Back-grounded Variations Corresponding to the Different Lenses

The regression functions were then brought to recover the distortions of the validation sets Lens#1 to Lens#4. Figure 8 shows these recovered $(\hat{x}_u, \hat{y}_u)$ of the validation sets by both the optimized SVR function and the algebraic polynomial regression. As shown, most of the recovered $(\hat{x}_u, \hat{y}_u)$ of the validation sets are inexact with respect to their corresponded (x_u, y_u). The inexactness even is extended to the training set Lens#5 itself. The fact behind the self-inexactness is due to the effort used to trade off the robustness we expected.

Instead the inexactness brought by the regressions, the key point we have to stress is the variation-resistant capability that the regressions can achieve. An examination of root mean square error (RMSE) was thus issued by the cross-validation (Table 1). As exhibited in this table, the calibration accuracies form SVR majorly are higher than those from the 2nd order algebraic polynomial regression except the accuracy

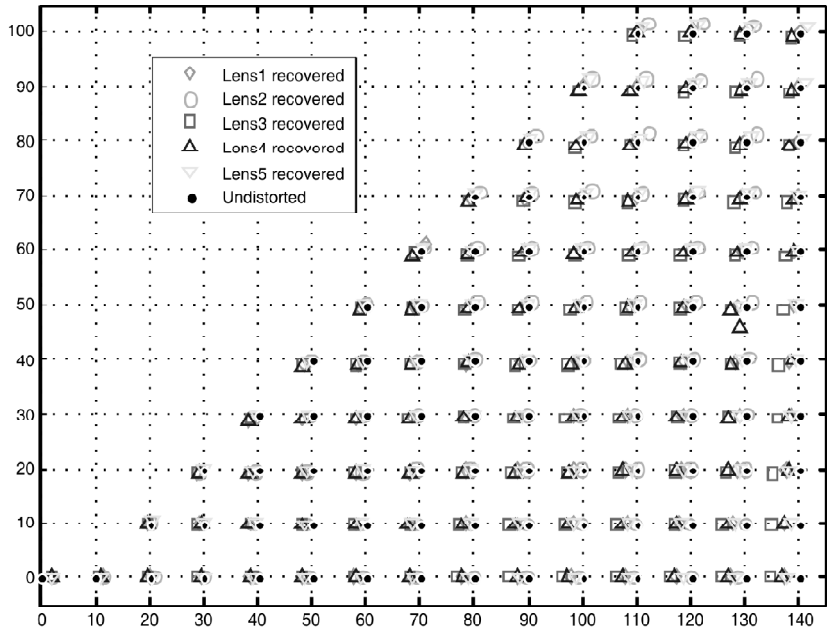

(a) Recovered by SVR

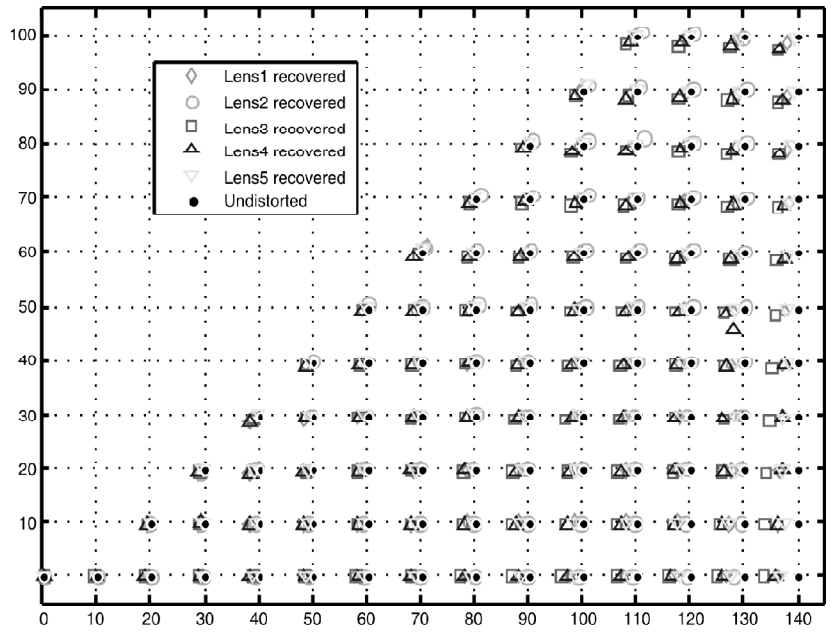

(b) Recovered by a 2nd order algebraic polynomial

Figure 8: Recovered Data Points $(\hat{x}_u, \hat{y}_u)$ with their Corresponded (x_u, y_u)

of the training set Lens#5. The higher accuracies from SVR satisfy the expectation, and assert the calibration by SVR a relatively higher robustness. As understanding, a model with high accuracy in a re-substitution validation of the training dataset is often overfitted. It means the low RMSE with the 2nd order algebraic polynomial regression would be too fitted to dataset Lens-5, and hence degraded the calibration capability in applying to the other datasets.

Table 1
Root Mean Square Error Comparison

RMSE (Root mean square error)	*Lens #1*	*Lens #2*	*Lens #3*	*Lens #4*	*Lens #5*
Recovered by SVR	1.44	1.05	2.43	2.21	1.14
Recovered by 2nd order algebraic polynomial	1.69	1.08	2.85	2.58	0.65

VI. CONCLUSIONS

Our proposed robust embedded lens calibrator by employing SVR has shown reliable results. With the proposal of a device-independent lens calibrator, the capability of robustness for the corresponding regression function is essentially needed. The study, with the evidence of a relatively high robustness, shows that SVR with its noise tolerability is an admissible candidate to develop the calibrator. Indeed, the tolerable capability is a key to achieve the calibration robustness. Although the preliminary validations feature the feasibility of such an application, a broad investigation and an in-depth systematic design should be complete in the future.

ACKNOWLEDGEMENT

This work was supported by grants from National Science Council, Taiwan, ROC under contracts NSC100-2221-E-149-002 and NSC100-2218-E-149-002. The authors would like to thank Chien-Kai Chen, Wun-Yi Lin, Yi-Hong Tu, and Hsing-Yu Pan for their remarkable help for the study.

REFERENCES

[1] G. Q. Wei, and S. D. Ma, "Implicit and explicit camera calibration: theory and 8 experiments," *IEEE Transaction on Pattern Analysis and Machine Intelligence*, Vol. 9 16, No. 5, pp. 469–480, 1994.

[2] T. A. Clarke, and J. F. Fryer, "The development of camera calibration methods 11 and models," *Photogrammetric Record*, Vol. 16, pp. 51–66, 1998.

[3] E. E. Hemayed, "A survey of camera self-calibration," *Proc. IEEE Conference on* 13 *Advanced Video and Signal Based Surveillance*, pp. 351–357, 2003.

[4] R. Y. Tsai, "An efficient and accurate camera calibration technique for 3d machine vision," *Proc. IEEE Conference on Computer Vision and Pattern Recognition*, pp. 364–374, 1986.

[5] R. Y. Tsai, "A versatile camera calibration technique for high-accuracy 3D machine vision metrology using off-the-shelf TV camera and lenses," *IEEE Journal of Robotics and Automation*, Vol. 3, No. 4, pp. 323–344, 1987.

[6] F. Devernay, and O. Faugeras, "Straight lines have to be straight: automatic calibration and removal of distortion from scenes of structured environments," Machine Vision and Applications, Vol. 1, pp. 14–24, 2001.

[7] H. Haneish, and Y. Miyake, "Distortion compensation of electronic endoscope images," *Proc. IEEE Conf Rec. Medical Image Conf.*, vol. 3, pp. 1717–1721, 1993.

[8] W. E. Smith, N. Vakil, and S. A. Maislin, "Correction of distortion in endoscope images," *IEEE Transaction on Medical Imaging*, Vol. 11, No. 1, pp. 117–122, 1992.

[9] Wikimedia Foundation, "Runge's phenomenon," http://en.wikipedia.org/wiki/Runge%27s_phenomenon, Wikipedia, 21 June 2012.

[10] C. Y. Yang, J. J. Chou, and F. L. Lian, "Robust classifier learning with fuzzy class labels for large-margin support vector machines," *Neurocomputing*, Vol. 99, pp. 1–14, 2013.

[11] V. N. Vapnik, *The Nature of Statistical Learning Theory*. New York: Springer-Verlag, 1995.

[12] V. N. Vapnik, *Statistical Learning Theory*. New York: John Wiley & Sons, 1998.

[13] C. J. Lin, "Formulations of support vector machines: a note from an optimization point of view," *Neural Computation*, Vol. 13, No. 2, pp. 307–317, 2001.

[14] B. Schölkoph, and A. J. Smola, *Learning with kernels*. Cambridge, MA: MIT Press, 2002.

[15] A. J. Smola, and B. Schölkopf, "A tutorial on support vector regression," *Technical Report*, NeuroCOLT, NC-TR-98-030, University of London, UK, 1998.